Available online at www.sciencedirect.com
SCIENCE DIRECT®
C. R. Physique 6 (2005) 739–748
COMPTES RENDUS PHYSIQUE
http://france.elsevier.com/direct/COMREN/

Neutrino Physics/Physique des neutrinos

Atmospheric neutrinos and neutrino oscillations

Takaaki Kajita [a,*], Paolo Lipari [b]

[a] *Research Center for Cosmic Neutrinos, Institute for Cosmic Ray Research, University of Tokyo, Kashiwa-no-ha 5-1-5, Kashiwa, Chiba 277-8582, Japan*

[b] *INFN and Dipartimento di Fisica, Università di Roma 1, P. A. Moro 2, 00185 Roma, Italy*

Available online 16 September 2005

Abstract

Atmospheric neutrinos are produced by the interaction of primary cosmic rays in the upper atmosphere. Their measurement with large underground detectors has given results that are inconsistent with predictions based on the Minimal Standard Model. The ν_e and $\bar{\nu}_e$ fluxes, within errors, are compatible with the standard prediction, while the ν_μ and $\bar{\nu}_\mu$ fluxes show a significant suppression. The dependence of the suppression on the neutrino energy and direction (path-length) can be accurately described assuming the existence of two flavor $\nu_\mu \leftrightarrow \nu_\tau$ oscillations with parameters in the (90% CL) allowed interval: $1.5 < |\Delta m^2|/(10^{-3}\ \mathrm{eV}^2) < 3.4$ and $\sin^2 2\theta \geqslant 0.92$. Various features of neutrino oscillations have been studied based on these data. ***To cite this article: T. Kajita, P. Lipari, C. R. Physique 6 (2005).***

Résumé

Les neutrinos atmosphériques et les oscillations de neutrinos. Les neutrinos atmosphériques sont produits par l'interaction des rayons cosmiques primaires dans les hautes couches de l'atmosphère. Leur détection avec des détecteurs massifs et souterrains donne des résultats incompatibles avec le modèle standard minimal de la physique des particules. Si le flux de ν_e et de $\bar{\nu}_e$ est en accord avec les prédictions, le flux de ν_μ et de $\bar{\nu}_\mu$ montre une suppression significative. La dépendence de cette suppression avec l'énergie et la distance parcourue (liée à la direction) des neutrinos peut être décrite avec précision par le mécanisme d'oscillation des neutrinos á deux saveurs $\nu_\mu \leftrightarrow \nu_\tau$. Les paramètres d'oscillation qui donnent le meilleur ajustement des données sont (à 90% CL) $1.5 < |\Delta m^2|/(10^{-3}\ \mathrm{eV}^2) < 3.4$ et $\sin^2 2\theta \geqslant 0.92$. Plusieurs caractéristiques de l'oscillation sont également étudiées. ***Pour citer cet article : T. Kajita, P. Lipari, C. R. Physique 6 (2005).***

Keywords: Atmospheric neutrinos; Neutrino oscillations; Super-Kamiokande

Mots-clés : Neutrinos atmosphériques ; Oscillation des neutrinos ; Super-Kamiokande

1. Introduction

Neutrinos are the only known electrically neutral fermions, and exist in three separate flavors, identified by the charged lepton (e, μ or τ) associated with the neutrino in charged current transitions. Neutrinos are much lighter than all other known fermions, and in fact all attempts to measure their mass have only yielded upper limits. However if neutrinos have non-vanishing

* Corresponding author.
E-mail addresses: kajita@icrr.u-tokyo.ac.jp (T. Kajita), paolo.lipari@roma1.infn.it (P. Lipari).

1631-0705/$ – see front matter
doi:10.1016/j.crhy.2005.07.004

masses, they are able to change their flavor during propagation. This phenomenon is known as neutrino (flavor) oscillations [1, 2]. In general, the neutrino states with well defined flavor: $\{\nu_e, \nu_\mu, \nu_\tau\}$ and the states with well defined mass: $\{\nu_1, \nu_2, \nu_3\}$ do not coincide. The two triplets can be seen as two orthonormal basis in the neutrino Hilbert space and are related by a unitary matrix U. As an example, the ν_μ state can be written as the superposition:

$$|\nu_\mu\rangle = U_{\mu 1}|\nu_1\rangle + U_{\mu 2}|\nu_2\rangle + U_{\mu 3}|\nu_3\rangle \tag{1}$$

Neutrinos are usually created in charged current (CC) interactions, and therefore in a flavor eigenstate. A neutrino created with flavor α and 3-momentum $\vec{p}$ will not have a well defined energy, since each one of the three mass components will have a different energy:

$$E_j = \sqrt{p^2 + m_j^2} \simeq p + \frac{m_j^2}{2p} \simeq E + \frac{m_j^2}{2E} \tag{2}$$

Each component will evolve in time acquiring a (slightly different) quantum phase with the result:

$$\big|\nu_\mu(t)\big\rangle = \sum_j U_{\mu j}|\nu_j\rangle \exp[-\mathrm{i}E_j t] \tag{3}$$

The tiny energy splits between the different components, after a sufficiently long time (or a sufficiently long distance $L \simeq ct$), will result in a large differences in phase, and the probability for flavor transition: $P(\nu_\mu \to \nu_\tau) \equiv |\langle \nu_\tau | \nu_\mu(t)\rangle|^2$ can in general become large.

For simplicity we will consider two-flavor oscillations, involving two flavors (ν_μ and ν_τ) and two mass eigenstates that we can choose to label ν_2 and ν_3. The mixing matrix reduces to the form:

$$U = \begin{pmatrix} \cos\theta_{23} & \sin\theta_{23} \\ -\sin\theta_{23} & \cos\theta_{23} \end{pmatrix} \tag{4}$$

with the mixing angle $\theta_{23} \in [0, \pi/2]$. The probability for a neutrino of energy E_ν, produced in flavor state ν_μ to be observed with the different flavor (ν_τ) at a distance L from its creation point is:

$$P(\nu_\mu \to \nu_\tau) = \sin^2 2\theta_{23} \sin^2\left(\frac{\Delta m_{23}^2 L}{4E_\nu}\right) \tag{5}$$

where $\Delta m_{23}^2 = m_3^2 - m_2^2$. In Eq. (5) we have used natural units ($\hbar = c = 1$); measuring Δm_{23}^2 in eV^2, L in km and E_ν in GeV, the factor $1/4$ in the argument of the second sin becomes 1.27. The flavor transition has a non negligible probability only if the mixing angle is not too small, (since it is proportional to $\sin^2 2\theta_{23}$) and when the neutrino mass eigenstates have accumulated a sufficiently large phase difference, that is when $L|\Delta m_{23}^2|/(4E_\nu) \gtrsim 1$. Therefore for a given E_ν, one needs a sufficiently long path-length L. More details on the oscillation mechanism can be found in [33].

Atmospheric neutrinos are produced when cosmic-ray protons and nuclei enter the atmosphere and interact generating different types of secondary particles, which in turn can interact or propagate to the ground (depending on the particle type and energy). The production of atmospheric neutrinos is schematically shown in Fig. 1. They have a very broad energy spectrum that extends from ~ 30 MeV up to very high energies. Neutrinos with energy below $E \lesssim 10^5$ GeV have a cross section sufficiently small, so that they can cross the Earth even when traveling along trajectories that traverse its center. This fact has the important consequence that an atmospheric neutrino detector is able to observe particles coming from all directions, that is both down-going neutrinos (produced in the atmosphere above the detector), and up-going neutrinos, that have been created in a different point on the Earth, have penetrated the interior of the Earth, and are exiting at the detector site. This situation is ideal for the study of flavor oscillations, because the neutrino path-length L can vary (depending on the neutrino direction at the detector) from $L_{\min} \simeq 10$ km for vertically down-going particles to $L_{\max} \simeq 2R_\oplus \simeq 1.25 \times 10^4$ km, and one can search for oscillation effects comparing the measurements for neutrinos that have traveled for different path-lengths.

In fact the measurements of atmospheric neutrinos of Super-Kamiokande (SK) [3,4] and other detectors [5–9] have provided strong evidence for the existence for neutrino oscillations. This evidence has been recently confirmed by the K2K long-baseline accelerator experiment [10]. Oscillations of longer path-lengths have also been observed with solar and reactor neutrinos [11–13]. These results are compatible with the atmospheric neutrino data, and together describe some remarkable patterns for the ν masses and mixings.

This work is intended as a brief review of the measurements of atmospheric neutrinos, and the interpretation of the results. It is organized as follows: in Sections 2 and 3 we describe the prediction of the atmospheric neutrino rates, and the detectors used for the measurements, in Section 4 we present the data and their interpretation in terms of neutrino oscillations. In Section 5 we discuss the use of atmospheric neutrinos to set limits on different neutrino properties. Finally, in the last section, we give a brief summary and discuss the perspectives for future studies.

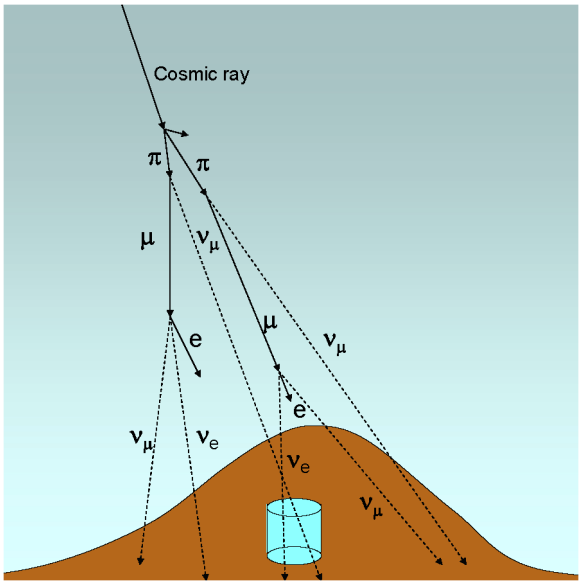

Fig. 1. A schematic view of the generation of neutrinos in the atmosphere. Cosmic ray particles interact with the air nucleus producing pions (and less frequently Kaons). A $\pi^+(\pi^-)$ decays to a $\mu^+(\mu^-)$ and a $\nu_\mu(\bar{\nu}_\mu)$. Subsequently, the $\mu^+(\mu^-)$ decays to an $e^+(e^-)$, a $\nu_e(\bar{\nu}_e)$ and a $\bar{\nu}_\mu(\nu_\mu)$.

2. Prediction of the atmospheric neutrino fluxes

The search for the possible existence of ν flavor oscillations implies the comparison of the data with theoretical predictions calculated with and without the presence of oscillations. The calculation of the atmospheric neutrino fluxes (for a complete discussion, see [16]) starts from a description of the Cosmic Ray (CR) spectrum on top of the atmosphere; then computes the distributions (in flavor, energy, and direction) of the neutrinos produced by the CR particles; finally the neutrinos are propagated from the production point to the detector. In the absence of oscillations this is trivial, in the general case one has to consider (as a function of the relevant parameters) the flavor transition probabilities.

The CR flux at the Earth has to be measured experimentally, and this implies the use of detectors placed on balloons or satellites. These are not easy measurements and their systematic errors (that result in discrepancies between different observations) are an important source the systematic error in the atmospheric neutrino calculation. Note that while the CR fluxes in interstellar space are (to a very good approximation) constant in time and isotropic in direction, at low rigidity (p/Z) the effects of the solar wind, (that varies with 11 years periodicity, and acts as a time varying source of energy loss for the CR) introduce a small time dependence, and the effects of the geomagnetic field break the CR isotropy. The geomagnetic field prevents the lowest rigidity particles from reaching the surface of the Earth. The geomagnetic effects vanish at the magnetic poles and are strongest at the magnetic equator (latitude effect) and, since CR have positive electric charge, are strongest for east-going particles (east–west effect). The geomagnetic effect is equivalent to the effect of a rigidity 'cutoff' $R_{\rm cut}(\vec{x}_\oplus, \Omega)$. The flux of CR from direction Ω at the position $\vec{x}_\oplus$ vanishes if $p/Z < R_{\rm cut}$, while it coincides with the unperturbed spectrum for larger rigidities. This result can be derived as a consequence of the propagation in a static magnetic field of a CR population that is isotropic at large distance from the Earth. For an exactly dipolar magnetic field the cutoff can be calculated analytically (the Stormer solution), for the real field and a more accurate calculations one has to study numerically the problem.

The second step in the ν flux estimate is the calculation of neutrino production in the development of hadronic showers. This task requires a detailed description of multi-particle production in strong interactions, and in addition careful propagation of secondary particles in the atmosphere taking into account energy losses (this is especially important for muons). It is well known that we are not able to compute from first principles the properties of particle production in the strong interactions, and one has to rely on experimental data collected at accelerators, interpolating (or extrapolating) when needed. This introduce another important source of systematic uncertainty in the calculation of the atmospheric neutrino flux.

To perform the calculation, analytic approximations exist, however the most accurate results are obtained with Monte Carlo methods. For maximum accuracy, one has to recur to a 'straightforward', but highly inefficient, method where showers of all (geomagnetically allowed) directions, are generated over the entire surface of the Earth testing if they produce neutrinos that intersect the detector (placed at its geographical position). This '3-Dimensional' method substitutes the less accurate, but computationally much simpler '1-Dimensional' method of older calculations, where the neutrinos are assumed to be collinear

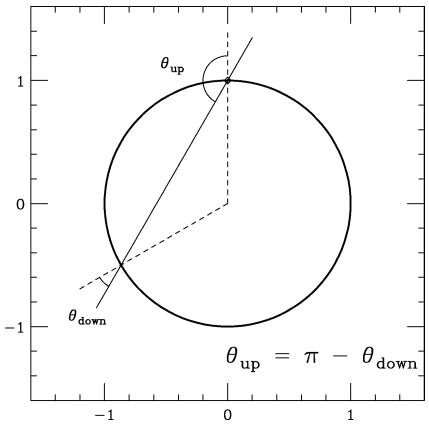

Fig. 2. A neutrino trajectory that enters a spherical Earth with zenith angle $\theta_{\rm in}$ will exit with a new zenith angle $\theta_{\rm out} = \pi - \theta_{\rm in}$. Assuming that the primary fluxes are equal at the entry and exit points (isotropy), one can deduce the up-down symmetry of the fluxes.

with the primary CR particle. This is in fact a good approximation for $E_\nu \gtrsim 2$ GeV, where the two methods give approximately equal results.

The main source of atmospheric neutrinos is the chain decay of charged pions:

$$\begin{array}{lll} \pi^+ \to \mu^+ + \nu_\mu & \qquad & \pi^- \to \mu^- + \bar{\nu}_\mu \\ \quad\downarrow & & \quad\downarrow \\ \quad e^+ + \nu_e + \bar{\nu}_\mu & & \quad e^- + \bar{\nu}_e + \nu_\mu \end{array} \tag{6}$$

(See Fig. 1.) Smaller sources are due to kaon decays. Eq. (6) tells us that the fluxes of ν_e, ν_μ's and antineutrinos are strictly related to each other, and in particular that, if the muon decay probability is equal to unity, one has:

$$\phi(\nu_\mu + \bar{\nu}_\mu) \simeq 2\,\phi(\nu_e + \bar{\nu}_e) \tag{7}$$

Eq. (7) is actually valid not only in an 'integral sense' but also as function of energy and angle, since the three neutrinos produced in the chain decay of a pion are approximately collinear and have similar average energies. With increasing energy, because of the Lorentz time dilatation, the muons begin to reach the ground before decay, and the ratio $r_\nu = (\nu_\mu + \bar{\nu}_\mu)/(\nu_e + \bar{\nu}_e)$ increases. It is important also to note that the flux of muons that reaches the ground (or that are present at high altitude where they can be measured by experiments on balloons) are also calculable, and the comparison of the calculations with the muon data is an important constraint that can reduce systematic uncertainties.

The essential point of this discussion is that value of the ratio r_ν can be predicted very robustly, independently from the details of the calculation. Early (and modern [17–19]) calculations of the ratio r_ν show difference $\lesssim 5\%$ (3%). The earliest evidence for the existence of oscillations for atmospheric neutrinos came in fact from the observation of a measured r_ν smaller that the prediction [5–7].

A second very robust result of the atmospheric ν calculation, is the prediction that in the absence of flavor transitions, the neutrino fluxes are to a very good approximation up-down symmetric, that is for every neutrino type:

$$\phi_{\nu_\alpha}(E, \cos\theta) = \phi_{\nu_\alpha}(E, -\cos\theta) \tag{8}$$

Eq. (8) can be derived as an elementary geometry theorem (see Fig. 2), from the assumptions isotropy of the CR, and sphericity of the Earth.

For the prediction of observable event rates (and not only fluxes), one has to include a description of the ν cross sections, that in the energy range $E_\nu \in [0.1, 10]$ GeV, have uncertainties of order 15%, and of course a detailed knowledge of the detector efficiency and acceptance.

3. Atmospheric neutrino experiments

The rate of atmospheric neutrino interactions is about 200 (kton yr)$^{-1}$. The background rate at the surface, mostly due to atmospheric muons, is so high that, with the present technology it has been possible to observe the atmospheric neutrinos only with detectors placed deep underground. Even underground, the problems of background rejection and identification of the neutrino-induced events have to be carefully studied. Events are accepted only if the ν interaction point is within a fiducial

volume that excludes the more external volume of the detector (to reject photon and neutron contaminations) and outer (or veto) detectors are set up, to test for the presence of entering or exiting charged particles.

For low neutrino energy, ν-events are selected requiring that they are 'fully contained' (FC), and all secondary particles remain inside the detector volume. In this case the background rejection is relatively easy, and is obtained requiring the absence of signals from the outer- (or veto-) detector, and requiring that the interaction vertex position is in a fiducial volume. The requirement that all particles are absorbed inside the detector volume limits this class of events to $E_\nu \lesssim$ few GeV. With increasing energy, the requirement of confinement for all particles reduces the detection efficiency, and in particular the muons produced by CC ν_μ and $\bar{\nu}_\mu$ interactions can easily exit from the detector volume. However, events where a clearly identified muon is the only exiting particle, can also be selected as neutrino events and are referred to as 'partially contained' (PC) events.

There is a third category of CC ν_μ events, where the interaction occurs outside the detector, and the muon enters and either passes through or stops in the detector. These are referred to as 'upward-going muons' because one generally requires they originate from below the horizon to ensure that a sufficient amount of rock absorbs ordinary cosmic ray muons. The median energies for upward stopping and through-going muon events are 10 and 100 GeV, respectively.

To date, two significantly different techniques, water Cherenkov and find grained tracking detectors, have been used to observe these atmospheric neutrino events.

3.1. Water Cherenkov detectors

In water Cherenkov detectors, an atmospheric neutrino event is detected by observing Cherenkov radiation from relativistic charged particles produced by the neutrino interaction with the nucleus. A two-dimensional array of photomultiplier tubes on the inside surface of the detector detects the photons. The hit time and the pulse height from each PMT are recorded. The timing information, with a typical resolution of a few ns for a single photo-electron pulse, is useful for reconstruction of the vertex position. The total number of photo-electrons gives information on the energy of the particles above Cherenkov threshold. Some of the water Cherenkov detectors are equipped with an anti-counter that surround the inner detector. In the 1980s and early 1990s, Kamiokande [5,6] and IMB [7] observed the early indication for atmospheric neutrino oscillations.

The current generation water Cherenkov detector is Super-Kamiokande, whose results dominate our understanding of atmospheric neutrinos. It began taking data in 1996. It has a total mass of 50 ktons. It uses 11 146 20-inch diameter PMTs, with photo-cathode coverage of 40% of the inner detector surface. An outer detector surrounds the inner detector with 2 m thickness of water, equipped with 1885 8-inch PMTs with wavelength shifting plates. The fiducial volume for neutrino vertices is 2 m from the plane of photomultiplier tubes, resulting in a 22.5 kton mass. The large mass and photo cathode coverage allow for high statistics and detailed studies of atmospheric neutrinos.

3.2. Fine grained tracking detectors

The second category of atmospheric neutrino detectors consists of comparatively fine resolution tracking detectors. Tracking detectors have an advantage in sensitivity because they can detect low momentum charged particles that would be below Cherenkov threshold in water. In the 1980s, the NUSEX [14] and Frejus [15] experiments studied atmospheric neutrino interactions in detail.

More recent experiment, Soudan-2 [8], is able to reconstruct the short and heavily ionizing trajectory of recoil protons from atmospheric neutrino events such as $\nu_\mu n \to \mu^- p$. The Soudan-2 detector is a 963 ton detector with the fiducial mass of 770 tons. It is equipped with anti-counters. The anti-counter is useful to estimate the fraction of non-neutrino background events in the atmospheric neutrino sample as well as to eliminate cosmic ray background events easily.

There is a second type of tracking detector, mostly sensitive to muon neutrinos in the form of upward-going muons. One example of such detector is MACRO [9], with a relatively large area ($\simeq 860$ m^2), and an absorber mass of $\simeq 0.8$ kton. This detector could identify the direction of the muon by resolving the time-of-flight as it traverses two or more layers of liquid scintillator. The MACRO detector is composed three horizontal planes with the lower section filled with crushed rock absorber and a hollow upper section. In addition to through-going muons, MACRO has analyzed partially contained and stopping muon topologies, where the crushed rock in the lower section acts as neutrino target or muon stopper, respectively.

4. Experimental results and oscillation analyses

To study neutrino oscillations, the flavor of the interacting neutrinos must be determined. This is only possible for CC interactions, identifying the charged lepton in the final state. Electrons with energy greater than ~ 100 MeV produce an electromagnetic shower in the detector material, while for muons below $E_\mu \sim 10^3$ GeV, the dominant source of energy loss is ionization, and a single particle propagates losing smoothly its energy. For very fine grained detectors the separation of e and

μ is a relatively straightforward task. For water Cherenkov detectors one can separate 'showers' (e) from 'tracks' (μ) from the patterns of the Cherenkov light rings that are formed by a stopping charged particle (in water photons are emitted at approximately 42° from the particle direction). An electron ring is fuzzier than a muon one, because it is in fact the superposition of many rings produced by many low-energy $e^{\pm}$ that have undergone multiple scattering.

In the following we will discuss results from three recent, major atmospheric neutrino experiments: Super-Kamiokande, Soudan-2 and MACRO. Super-Kamiokande has observed more than 15 000 atmospheric neutrino events, and with these high statistics has given the dominant contribution to the observations. Fig. 3 (top) shows the zenith angle distributions for various data samples from Super-Kamiokande [4]. In order to predict the characteristics of the data, detailed Monte Carlo programs have been developed. The box histograms in Fig. 3 (top) show the predicted distributions without neutrino oscillations. It is clear that the number of up-going ν_μ events has deficit compared with the Monte Carlo prediction. Furthermore, the deficit of up-going ν_μ events has energy dependence. In the lowest energy range, the zenith angle dependence in the deficit is not visible. This is due to the poor angular correlation between the neutrino and lepton direction.

Consistent results have been obtained from the analyses of the contained events in Soudan-2 [8] and the upward-going muons and PC events in MACRO [9], see Fig. 3 (middle and bottom).

4.1. 2 flavor oscillation analysis

Data samples, which include significant CC ν_μ events shows zenith angle and energy dependent deficit of events. On the other hand, the zenith angle distributions for e-like data show no evidence for deviation from the predicted shape, and hence there is no evidence for the oscillations involving ν_e (see Fig. 3). Therefore, $\nu_\mu \to \nu_\tau$ oscillation is assumed to fit to the data. In this analysis, simulated neutrino events are oscillated according to Eq. (5), where $\sin^2 2\theta_{23}$ and Δm^2_{23} are the parameters to be estimated by the fit.

There are various sources of the systematic errors in the measurement and prediction. The dominant sources are the neutrino flux, the neutrino interaction cross sections and the detection efficiencies for CC ν_e and ν_μ interactions. These errors are carefully evaluated and are taken into account in the fitting. For example, in Super-Kamiokande, 39 systematic error terms are considered in the analysis. The allowed regions of $\nu_\mu \to \nu_\tau$ oscillation parameters from these experiments are shown in Fig. 4. The allowed regions from these experiments agree well. The 90% C.L. allowed region from Super-Kamiokande is $1.5\times10^{-3} < \Delta m^2_{23} < 3.4 \times 10^{-3}\mathrm{eV}^2$ and $\sin^2 2\theta_{23} > 0.92$.

Also shown in Fig. 4 is the allowed parameter region from the K2K long–baseline experiment [10]. K2K is the first long-baseline neutrino oscillation experiment. Neutrinos are produced using a proton beam accelerated by the KEK 12 GeV proton synchrotron, and are detected in Super-Kamiokande, which is 250 km away from KEK. This experiment observed 107 neutrino events, while the expected number of events was 151^{+12}_{-10}. In addition, the observed neutrino energy spectrum agreed with the oscillation prediction. The K2K data are consistent with neutrino oscillations. The allowed regions from atmospheric and long baseline experiments agree well.

The result that a neutrino mixing angle is large, was very unexpected, and is in sharp contrast with the situation for the quark sector, where all mixing angles are small. Moreover the mixing parameter ($\sin^2 2\theta_{23}$) is near to its maximal value. A maximal mixing would imply some 'special' reason like the existence of new symmetry, and the measurement of a (possible) deviation of θ_{23} from 45° is an important goal for future studies.

4.2. 3 flavor oscillation analysis

The general formula for flavor oscillations is complex, and involves two independent squared mass differences Δm^2_{12} and Δm^2_{23}, three mixing angles θ_{12}, θ_{13} and θ_{23}, and one CP violating phase δ. The measurements of solar and reactor neutrinos [11–13] have actually allowed one to determine a precise measurement of $\Delta m^2_{12} = 7.9^{+0.6}_{-0.5} \times 10^{-5}$ eV^2, and $\theta_{12} \simeq (32.3 \pm 2.5)^\circ$.

The 'solar' squared mass difference Δm^2_{12} is approximately 30 times smaller than $|\Delta m^2_{23}|$, and generates oscillations with a 30 times longer period. It is therefore a reasonable approximation to neglect the effects of Δm^2_{12} for atmospheric neutrinos. Even with this simplifying assumption, the oscillation probabilities will depend on the additional mixing angle θ_{13}, and in general the transitions $\nu_e \leftrightarrow \nu_\mu$ and $\nu_e \leftrightarrow \nu_\tau$ will be present, vanishing only in the limit $\theta_{13} \to 0$. Note that if ν_e are involved in the oscillations one has to take into account the presence of matter along the neutrino trajectory [26,27].

A three-flavor analysis of the SK data, shows that the data favors $\theta_{13} \simeq 0$ and sets an upper limit for this mixing angle. The sensitivity of an atmospheric neutrino detector for oscillations of ν_e is reduced because one has to consider both appearance ($\nu_\mu \to \nu_e$) and disappearance ($\nu_e \to \nu_\mu$, $\nu_e \to \nu_\tau$) channels, with a cancellation effect.

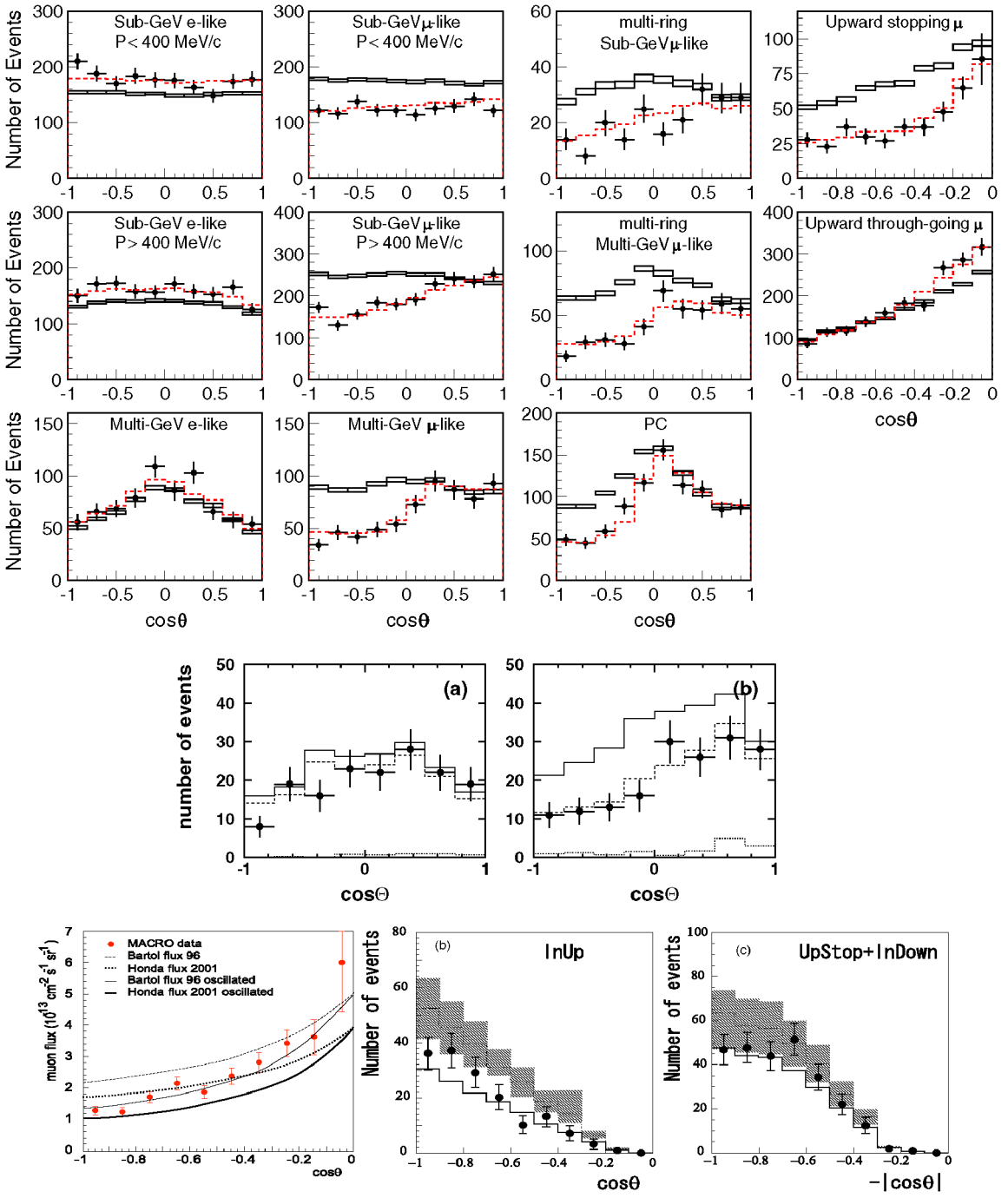

Fig. 3. Zenith angle distributions for atmospheric neutrino events observed in Super-Kamiokande (top), Soudan-2 (middle, (a) e-like, (b) μ-like) and MACRO (bottom, left: through-going muon flux, middle: upward-going PC events, right: upward-going stopping muons + downward-going PC events). $\cos\Theta = 1$ (-1) means down-going (up-going). The histograms show the prediction with and without $\nu_\mu \to \nu_\tau$ oscillations.

The constraint on θ_{13} from a study of the disappearance of $\bar{\nu}_e$ produced in nuclear reactors with a 1 km path-length (Chooz experiment [21]) gives a more stringent upper limit on θ_{13}. The result, in turn, implies that the 2-flavor oscillation analysis described in the previous section is approximately correct.

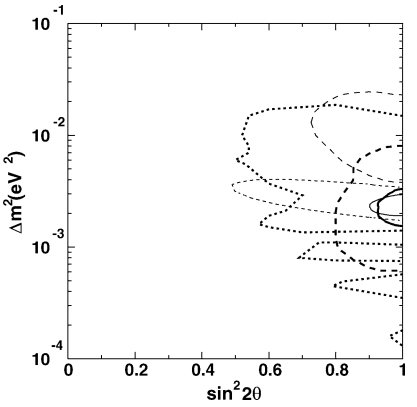

Fig. 4. 90% C.L. allowed neutrino oscillation parameter regions for $\nu_\mu \to \nu_\tau$ from atmospheric neutrino experiments: Kamiokande [20] (thin dashed line), Soudan-2 [8] (thick dotted line), MACRO [9] (thick dashed line), and Super-Kamiokande [4] (thick line). The allowed region from the L/E analysis in Super-Kamiokande is shown by the thin line. The thin dotted line shows the allowed region from K2K [10].

The possibility that the observed disappearance of the of the ν_μ, is due to transitions into a super-weakly interacting singlet [under $SU(2) \otimes U(1)$] particle (or a 'sterile' neutrino), has also been proposed and investigated. This possibility has been first excluded as the dominant mechanism [23], and is now also strongly constrained as a sub-dominant effect.

4.3. L/E analysis

Although Fig. 3 shows a clear zenith angle and energy dependent deficit of ν_μ events, these plots do not show any direct evidence for sinusoidal ν_μ survival probability of Eq. (5). This can be explained as a consequence of the poor resolution in L/E of the measurement, and the averaging over the oscillations. However other models, such as the neutrino decay [24] or the decoherence [25] models, can reasonably reproduce the observed atmospheric neutrino data with smooth (non-oscillating) probabilities. It is an important goal to confirm the validity of the oscillating form of Eq. (5). The first evidence that the ν_μ survival probability obeys a sinusoidal function has been recently obtained by Super-Kamiokande [22]. Neutrino events with good (better than 70%) resolution in L/E were selected. Then the event rate normalized by the prediction as a function of L/E was studied comparing with different predictions (see Fig. 5(left)). The oscillation prediction gives the best fit to the data reproducing the expected minimum at $L/E \simeq \pi|\Delta m^2| \simeq 500$ km/GeV. The neutrino oscillation parameters can be determined by the L/E distribution. The results for the allowed region are shown in the bottom part of Fig. 5. Note how the identification of the dip allows an accurate determination of Δm^2.

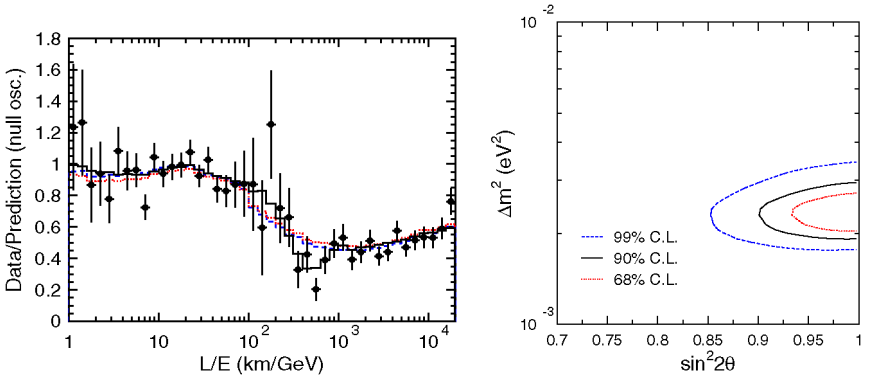

Fig. 5. Left: (Number of μ-like events)/(predicted number of μ-like events without oscillation) as a function of L/E from Super-Kamiokande. Only high L/E resolution FC + PC events were used. The solid, dashed and dotted histograms show the best-fit expectation for 2-flavor $\nu_\mu \leftrightarrow \nu_\tau$ oscillations, neutrino decay and neutrino decoherence, respectively. Right: 68, 90 and 99% allowed $\nu_\mu \to \nu_\tau$ oscillation parameter regions obtained by the L/E analysis.

5. Constraints on neutrino properties

The 'standard' mechanism described above involving neutrino masses and mixing is not the only one that results in flavor oscillations. In fact ν flavor transitions can also be generated by a variety of forms of non-standard neutrino interactions or properties that modify the Hamiltonian. One example of such non-standard interactions is the proposal [28] that different neutrino types could have different coupling to the gravitational field. Such difference is a violation of the Equivalence Principle (VEP) in General Relativity. In the VEP scenario (considering for simplicity only two flavors) the gravitational energy of neutrinos ν_1^G and ν_2^G (connected to the flavor eigenstates by the mixing angle θ_G) is $-2|\phi|E_\nu(1+\gamma_{1,2})$, where $\phi=-|\phi|$ is the gravitational potential, and $\gamma_1\neq\gamma_2$ are extra non-standard couplings. Much in the same way as for standard oscillations, even if the neutrinos are massless, one will have flavor transitions, because of the difference in phase: $2|\phi|\Delta\gamma E_\nu L$ accumulated between the two G-eigenstates. The corresponding flavor transition probability is:

$$P^{\mathrm{G}}_{\nu_\mu\to\nu_\tau}=\sin^2(2\theta_G)\sin^2[\Delta\gamma|\phi|E_\nu L] \tag{9}$$

A striking property of (9) is that the argument of the oscillating term, is proportional to LE_ν in contrast to the standard mechanism, where it is proportional to L/E_ν.

Flavor transitions of form (9) are also predicted in models (that violate Lorentz Invariance) where different particles have different asymptotic ($p\to\infty$) velocities [29], after the substitution $2|\phi\Delta\gamma|\leftrightarrow|\Delta v|$.

A different mechanism that can generate flavor transition [27] is the existence of flavor changing neutral currents (FCNC), that is processes like $\nu_\alpha+f\to\nu_\beta+f$ (with $\alpha\neq\beta$ and f a target fermion). The existence of these new interactions introduces additional non diagonal terms in the effective Hamiltonian for ν propagating in matter:

$$H^{\mathrm{FCNC}}_{\mu\tau}=H^{\mathrm{FCNC}}_{\tau\mu}=\frac{G_F}{\sqrt{2}}\varepsilon N_f \tag{10}$$

where ε is the ratio between the strengths of the new (FCNC) and standard (diagonal) NC interactions, and N_f is the density of fermion f. Extra non-universal neutral current interactions can also introduce a difference $H^{\mathrm{mat}}_{\mu\mu}-H^{\mathrm{mat}}_{\tau\tau}=G_F\varepsilon' N_f/\sqrt{2}$. These effects generate (for massless ν) a flavor transition probability:

$$P^{\mathrm{FCNC}}_{\nu_\mu\to\nu_\tau}=\frac{4\varepsilon^2}{4\varepsilon^2+\varepsilon'^2}\sin^2\left[\frac{G_F}{\sqrt{2}}X_f\sqrt{4\varepsilon^2+\varepsilon'^2}\right] \tag{11}$$

where X_f is the column density crossed by the neutrino. These effects have been proposed as an explanation of the atmospheric neutrino data; however, they are now all excluded as the dominant source of the observed effects [30]. It is, however, natural and interesting to study the possibility of the existence of these effects as *sub-dominant* contributions to the observations. It turns out that these effects are strongly restricted even at the sub-dominant level [31,32]. The inclusion of VEP effects is limited to $|\phi\Delta\gamma|\leqslant 4.0\times10^{-25}$; for FCNC $|\varepsilon_{\mu\tau}|\leqslant 0.034$. These limits may be the strongest constraints on these forms of New Physics beyond the standard model. Atmospheric neutrinos span several decades in E_ν and L, and therefore are very sensitive to these forms of new physics.

6. Summary

The experimental study of atmospheric neutrinos has lead to the discovery of neutrino oscillations. The first 'hints' of the existence of new physics were the measurement of a small ν_μ/ν_e ratio, and then the observation of a zenith angle dependence for the suppression. The high statistics data from Super-Kamiokande has allowed us to study in detail the energy and angular distributions of different flavor neutrinos, confirming the previous hints, and providing a robust demonstration of the dominant $\nu_\mu\leftrightarrow\nu_\tau$ standard oscillations, and determining the oscillation parameters. All alternative mechanisms proposed to reconcile data and predictions have been excluded. The recent L/E analysis from Super-Kamiokande, showing that the ν_μ disappearance probability obeys the sinusoidal form in L/E predicted by neutrino oscillations has played an important role in this exclusion.

The study of solar and reactor neutrinos [11–13] has also lead to the discovery of ($\nu_e\leftrightarrow\nu_{\mu,\tau}$) oscillations with a longer path-length. The solar and atmospheric results are perfectly consistent with each other, and a consistent pattern for the ν masses and mixing is emerging. The smallest mass splitting between mass eigenstates (Δm^2_{12}) controls the solar neutrino effects and the KamLAND data, while the larger squared mass difference measured with atmospheric neutrinos corresponds to $|\Delta m^2_{23}|\simeq|\Delta m^2_{13}|$. The mixing angles measured with solar and atmospheric neutrinos correspond to θ_{12} and θ_{23}, respectively. Note that there is an ambiguity in the ordering of the mass eigenstates. The 'most isolated' mass eigenstates (ν_3), that appears to be a superposition of ν_μ and ν_τ with approximately the same weight, could be either the heaviest (normal hierarchy) or the lightest (inverse hierarchy) neutrino. This is one of the open problems for the future, together with the measurements of the two remaining parameters in the mixing matrix; the angle θ_{13} (for which there is only an upper limit), and the CP-violating

phase δ. The absolute value of the neutrino masses is not accessible with flavor transition measurements, but can be studied with cosmological observations or (if neutrinos are Majorana particles) by searching for double beta decay.

The study of the flavor oscillations controlled by $|\Delta m^2_{23}|$ is accessible with long baseline (LBL) accelerator neutrino beams, and several large scale LBL projects are planned for the near (and not so near) future, with the goal to obtain more precise measurements of the known parameters, and complete our knowledge of the neutrino masses and mixing.

Atmospheric neutrino experiments have unique features, such as well understood and precisely predicted properties such as flavor and up-down ratios, and especially a wide coverage of the neutrino energy and path-length. Because of this feature, atmospheric neutrino experiments are likely to give a significant contributions to future neutrino oscillation studies especially if new large mass detectors will become available to obtain larger statistics. Moreover, the feature is ideal for the study of sub-dominant effects due to extra-dynamics in the Hamiltonian. Thus, the scientific potential of future atmospheric neutrino experimental studies remains of great interest.

Acknowledgements

One of the authors (TK) has been supported by the Japanese Ministry of Education, Culture, Sports, Science and Technology and by Japan Society for the Promotion of Science.

References

[1] Z. Maki, M. Nakagawa, S. Sakata, Prog. Theor. Phys. 28 (1962) 870.
[2] B. Pontecorvo, Zh. Eksp. Teor. Fiz. 53 (1967) 1717, Sov. Phys. JETP 26 (1968) 984.
[3] Y. Fukuda, et al., Super-Kamiokande, Phys. Rev. Lett. 81 (1998) 1562.
[4] Y. Ashie, et al., Super-Kamiokande, hep-ex/0501064.
[5] K.S. Hirata, et al., Kamiokande, Phys. Lett. B 205 (1988) 416;
K.S. Hirata, et al., Kamiokande, Phys. Lett. B 280 (1992) 146.
[6] Y. Fukuda, et al., Kamiokande, Phys. Lett. B 335 (1994) 237.
[7] D. Casper, et al., IMB, Phys. Rev. Lett. 66 (1991) 2561;
R. Becker-Szendy, et al., IMB, Phys. Rev. D 46 (1992) 3720.
[8] M.C. Sanchez, et al., Soudan-2, Phys. Rev. D 68 (2003) 113004.
[9] M. Ambrosio, et al., MACRO, Euro. Phys. J. C 36 (2004) 323.
[10] E. Aliu, et al., K2K, Phys. Rev. Lett. 94 (2005) 081802.
[11] M.B. Smy, et al., Super-Kamiokande, Phys. Rev. D 69 (2004) 011104;
S.N. Ahmed, et al., SNO, Phys. Rev. Lett. 92 (2004) 181301.
[12] T. Araki, et al., KamLAND, Phys. Rev. Lett. 94 (2005) 081801;
K. Eguchi, et al., KamLAND, Phys. Rev. Lett. 92 (2004) 071301.
[13] M. Cribier, T. Bowles, C. R. Physique 6 (2005).
[14] M. Aglietta, et al., NUSEX, Europhys. Lett. 8 (1989) 611.
[15] Ch. Berger, et al., Frejus, Phys. Lett. B 227 (1989) 489;
Ch. Berger, et al., Frejus, Phys. Lett. B 245 (1990) 305.
[16] T.K. Gaisser, M. Honda, Annu. Rev. Nucl. Part. Sci. 52 (2002) 153.
[17] M. Honda, T. Kajita, K. Kasahara, S. Midorikawa, Phys. Rev. D 70 (2004) 043008.
[18] G.D. Barr, T.K. Gaisser, P. Lipari, S. Robbins, T. Stanev, Phys. Rev. D 70 (2004) 023006.
[19] G. Battistoni, A. Ferrari, T. Montaruli, P.R. Sala, Astr. Phys. 19 (2003) 269 (Erratum p. 291).
[20] S. Hatakeyama, et al., Kamiokande, Phys. Rev. Lett. 81 (1998) 2016.
[21] M. Apollonio, et al., Chooz, Phys. Lett. B 466 (1999) 415.
[22] Y. Ashie, et al., Super-Kamiokande, Phys. Rev. Lett. 93 (2004) 101801.
[23] S. Fukuda, et al., Super-Kamiokande, Phys. Rev. Lett. 85 (2000) 3999.
[24] V. Barger, et al., Phys. Lett. B 462 (1999) 109.
[25] E. Lisi, et al., Phys. Rev. Lett. 85 (2000) 1166.
[26] S.P. Mikheyev, A.Yu. Smirnov, Sov. J. Nucl. Phys. 42 (1985) 1441;
S.P. Mikheyev, A.Yu. Smirnov, Nuovo Cimento C 9 (1986) 17.
[27] L. Wolfenstein, Phys. Rev. D 17 (1978) 2369.
[28] M. Gasperini, Phys. Rev. D 38 (1988) 2635.
[29] S.R. Coleman, S.L. Glashow, Phys. Lett. B 405 (1997) 249;
S.L. Glashow, et al., Phys. Rev. D 56 (1997) 2433.
[30] P. Lipari, M. Lusignoli, Phys. Rev. D 60 (1999) 013003, hep-ph/9901350.
[31] G.L. Fogli, E. Lisi, A. Marrone, G. Scioscia, Phys. Rev. D 60 (1999) 053006.
[32] M.C. Gonzalez-Garcia, M. Maltoni, Phys. Rev. D 70 (2004) 033010.
[33] J. Bouchez, C. R. Physique 6 (2005), in this issue.